Design of Fano Broadband Reflectors on SOI

Zexuan Qiang, *Member, IEEE*, Hongjun Yang, *Student Member, IEEE*, Santhad Chuwongin, Deyin Zhao, Zhenqiang Ma, *Member, IEEE*, and Weidong Zhou, *Senior Member, IEEE*

***Abstract*—We report here the design of Fano resonance broadband reflectors based on two-dimensional photonic crystals on silicon-on-insulator. The impact of vertical confinements and buffer configurations was investigated with a three-dimensional finite-difference time-domain technique. Spectral red- and blue-shifts were obtained by controlling the effective buffer layer indices, with very good agreement between experimental and simulation results.**

***Index Terms*—Broadband reflectors (BBRs), Fano resonances, integrated optics, photonic crystals (PCs).**

I. Introduction

COMPACT broadband reflectors (BBRs) are of great importance for optoelectronic devices and photonic integrated circuits like lasers, photodetectors, solar cells, and sensors, etc. [1]–[4]. Traditionally, they can be realized by using metal films or stacked dielectric thin films. Metal films can offer larger reflection bandwidth but are limited by the intrinsic absorption losses. Stacked dielectric thin films can achieve very low losses. But they typically require many individual layers with stringent refractive index and thickness tolerances for each layer. Recently, BBRs based on Fano resonance [5], or guided mode resonance [6], [7], have attracted great attention [8]–[15], where high reflections can be obtained with a single-layer one-dimensional (1-D) grating, or a two-dimensional photonic crystal slab (2-D PCS) structure. Owning to the strong interactions between in-plane guided modes and vertical radiation modes, Fano resonances occur with extremely high reflections. By properly controlling the design parameters, very broadband reflectors can be obtained. Various approaches have been reported to control the spectra performance of Fano BBRs, including stacked thin films [8], [9], [14], and binary grating [13], etc. Recently, we have also experimentally demonstrated postfabrication resonance control [15]. The postfabrication resonance control process we reported earlier can offer dynamic control. However, there exists saturation behavior in resonance shifts, as well as certain reflection degradations. Additionally, in practical BBR designs, the thickness of the low index buffer layers, as well as potential impact of substrate, needs to be investigated. In this letter, we attempt to address these BBR design issues by presenting detailed theoretical and simulation results. We consider different vertical confinement configurations. The simulation results were also compared with experimental data [15].

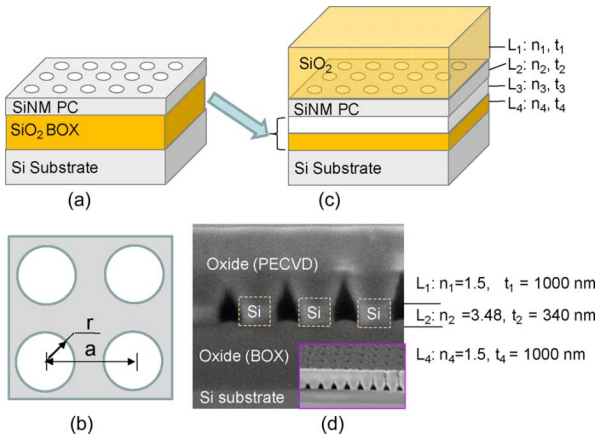

Fig. 1. (a) Basic Fano BBR structure based on SiNM PC on SOI substrate; (b) top view of square lattice PC structure with key lattice parameters defined as the air hole radius r and lattice constant a; (c) variations of Fano BBRs with core device layer (L_2: SiNM PC) surrounded by a combination of low index buffer layers (L_1, L_3, L_4); and (d) an SEM image of a Fano BBR fabricated, with PECVD oxide deposited on top of the patterned SiNM PCs. A 3-D SEM image is shown in the inset of (d).

In what follows, we first introduce a generic structure of Fano BBR based on postfabrication technique. Subsequently, we consider the impact of substrate and analyze two types of Fano BBRs, for both spectral resonance blue- and red-shifts, by effectively reducing the index layer below Si device layer and increasing the index layer above Si device layer, respectively. Finally, a conclusion is given.

II. Device Structure and Design

A basic Fano photonic crystal (PC) BBR is shown schematically in Fig. 1(a), where a patterned Si nanomembrane (SiNM) PC structure is formed on the top of the buried oxide (BOX) layer on a Si substrate. As shown in Fig. 1(b), a square lattice air hole PC structure is considered here for a reflection band around 1500 nm, with air hole radius r of 274 nm and lattice constant a of 980 nm. The thickness of the SiNM PC layer is 340 nm.

In our design here, we consider the impact of vertical buffer layers above and below the SiNM PC layer. A generic structure is then shown schematically in Fig. 1(c), where layer one

Manuscript received February 19, 2010; revised April 07, 2010; accepted May 08, 2010. Date of publication May 24, 2010; date of current version July 02, 2010. This work was supported in part by the U.S. AFOSR MURI program under Grant FA9550-08-1-0337, by the AFOSR under Contract FA9550-09-C-0200, and by the ARO under Grant W911NF-09-1-0505.

Z. Qiang was with the Department of Electrical Engineering, University of Texas at Arlington, Arlington, TX 76019-0016 USA, and also with the School of Physics and Optoelectronics Technology, Fujian Normal University, Fuzhou 350007, China (e-mail: qiangzx@fjnu.edu.cn).

H. Yang, S. Chuwongin, D. Zhao, and W. Zhou are with the NanoFAB Center, Department of Electrical Engineering, University of Texas at Arlington, TX 76019-0016 USA (e-mail: wzhou@uta.edu).

Z. Ma is with Department of Electrical and Computer Engineering, University of Wisconsin-Madison, WI 53706 USA (e-mail: mazq@engr.wisc.edu).

Color versions of one or more of the figures in this letter are available online at http://ieeexplore.ieee.org.

Digital Object Identifier 10.1109/LPT.2010.2050471

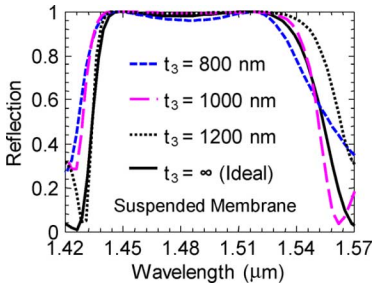

Fig. 2. Simulated reflection spectra for suspended membrane BBRs with different separation air gaps between the SiNM PC layer and the high index Si substrate.

with index n_1 and thickness t_1 is modified from air to oxide (or other index materials), denoted as $L_1 : n_1, t_1$. Additionally, the original BOX layer below the SiNM PC layer is partially etched away, which results in effectively a bilayer structure of air (denoted as $L_3 : n_3, t_3$) and oxide (denoted as $L_4 : n_4, t_4$).

III. Numerical Results and Discussion

For simplicity and numerical expediency, we limit the study to surface normal incidence. We also assumed the size of the designed pattern infinite. The design is then based on three-dimensional finite-difference time-domain (3-D FDTD) technique where the refractive indices of Si and SiO_2 used in the simulation are 3.48 and 1.45, respectively.

A. Impact of Substrate

We first consider the suspended membrane BBR structure on the top of the Si substrate, that is $t_1 = t_4 = 0$. As shown in Fig. 2, by reducing the air gap separation t_3, the simulated BBR reflection spectra experiences performance degradation, especially for the separation of less than 1000 nm. This is mostly related to the mode coupling between Fano resonances in the SiNM PC region and the substrate Si region. So a minimal of 1000-nm-thick separation is needed between SiNM PC layer and the Si substrate. In fact, we choose silicon-on-insulator (SOI) wafers with BOX layers of 1000 or 2000 nm for our study here. This shall ensure the decoupling of Fano resonance mode between the SiNM PC layer and the bottom Si substrate layer.

B. Effective Index Increase for Spectral Red-Shift

We then introduce the L_1 layer, e.g., to add SiO_2 via plasma-enhanced chemical vapor deposition (PECVD), on the top of the SiNM PC layer. The simulated reflection spectra intensity contour is shown in Fig. 3(a), with the structure under consideration also shown schematically in the inset of Fig. 3(b). For top deposited oxide thicknesses t_1 of 0 to 600 nm, a red-shift of ~40 nm was obtained, while the peak reflection remains almost unchanged, around 99%. Additionally, the reflection bandwidth improved for oxide thickness beyond 120 nm. This could contribute to a more symmetric field distribution along the vertical direction (LHLH), due to the presence of top oxide.

Another important factor we need to consider is the partial filling of oxide inside the air holes of SiNM PC layer. This is evident from the experimental results, as shown in Fig. 1(d), where a cross-sectional view of devices fabricated reveals partial filling of oxide inside the holes during the PECVD oxide

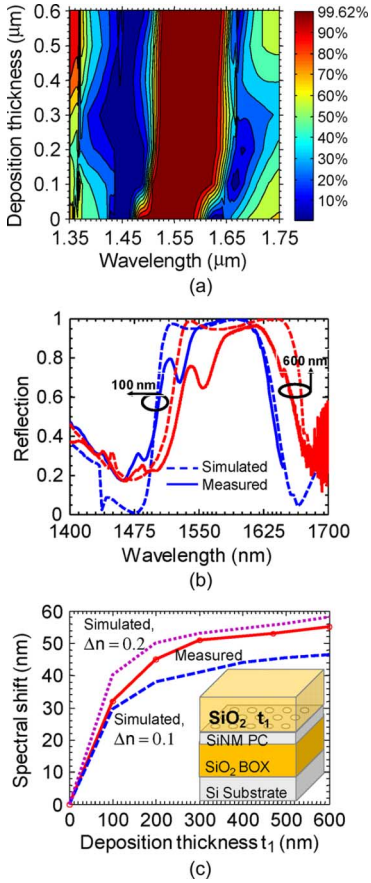

Fig. 3. (a) Simulated reflection intensity contour for BBRs with oxide deposited on top of the surface; (b) measured and simulated BBR reflection spectra with top oxide thicknesses of 100 and 800 nm, respectively; and (c) center wavelength shifts with the increase of the SiO_2 deposited on top of the SiNM PC layer. Δn on the simulation plots denotes the effective index increase inside the air hole region of SiNM PCs, due to partial filling/deposition of SiO_2 into the holes during the PECVD deposition process. Shown in the inset is a schematic of the structure under consideration here.

deposition process. This partial filling of oxide inside air holes will increase the average index L_3 layer and can lead to additional spectral-shift, as well as potentially degraded reflector performance. In our simulation results, we considered an average index increase of $\Delta n = 0.1$ in the air hole regions of SiNM PC layer (i.e., index for air holes increases from $n = 1.0$ to $n = 1.1$). The measured and simulated reflection spectra are shown in Fig. 3(b). The center wavelengths for the reflection bands are plotted in Fig. 3(b), along with the experimental results, obtained by depositing PECVD oxide with different thicknesses. It was noted that the simulation result agrees well with the experimental one, only for PECVD oxide thickness up to 100 nm. A larger spectral shift was observed experimentally, which indicates more oxide filling into air holes. By increasing the average index of air holes to $n = 1.2$ ($\Delta n = 0.2$), we see a much better fit between the experimental result and the simulation one. This indicates the strong impact of partial filling of oxide into the air holes, which can lead to larger spectral shift.

It is also worth noting that since the Fano resonance field is highly localized within 100 nm of high-index SiNM PC layer, we expect larger spectral-shift for the initial 100-nm oxide deposition. Further increase in the oxide thickness can only lead to a smaller change in resonance spectral-shift.

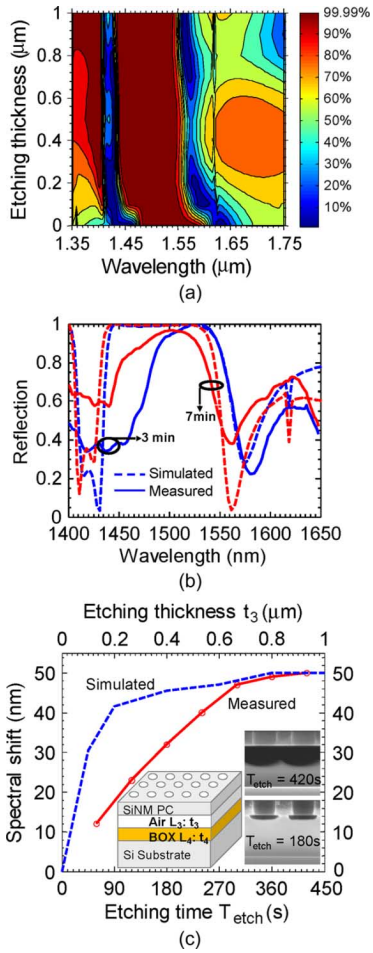

Fig. 4. (a) Simulated reflection intensity contour for BBRs with oxide BOX layer below partially etched away; (b) measured and simulated BBR reflection spectra for different etching times; and (c) center wavelength shifts with the increase of the air gap layer t_3. A schematic of the structure is shown in the inset, along with two cross-sectional SEM images of actual Fano BBR structures processed.

C. Effective Index Decrease for Spectral Blue-Shift

Finally, we can consider another case, where bottom BOX was partially etched away. The results are shown in Fig. 4, with the structure under consideration shown in the inset of Fig. 4(c). Since the total thickness of layer 3 (air, t_3) and layer 4 (SiO_2, t_4) should equal to the original BOX layer thickness (1000 nm used here), we scan the air thickness (t_3, or etching thickness). The simulated reflection spectra intensity contour is shown in Fig. 4(a). For air gap thickness from 0 to 1 μm (complete BOX layer removal), a blue-shift of $\sim$50 nm was obtained, as also shown in Fig. 4(c). Similar to the discussions before, we can achieve very large spectral-shift for the initial 100-nm air gap region.

The experimental results are also shown in Fig. 4(b), (c). Notice in this case, we can obtain excellent agreement between simulation and experiment with larger etching (air gap) thicknesses ($t_3 > 650$ nm). For smaller air gaps, the simulation results show larger spectral shift. This could be caused by the differences between simulation setup and experimental etching profiles. During the simulations, we consider a simple planar bilayer configuration (air L_3 and oxide L_4). However, the actual etching profiles are more complicated, especially for the initial etching thicknesses. Cross-sectional scanning electron micrograph (SEM) images for the structures at different etching times are shown in the inset of Fig. 4(b). For larger etching times ($T_{\rm etch} = 420$ s), the profile is closely matched with a bilayer approximation. However, for shorter etching times (e.g., $T_{\rm etch} = 180$ s), the isotropic etching leads to incomplete etching on the structure. This results in a much smaller resonance spectral-shift for smaller etching times.

IV. Conclusion

We report here the design of the Fano resonance BBRs on SOI substrate. High reflection BBRs with broadband spectral width is feasible, with optimized design of lattice parameters, and the desired separation between Si PC layer and the high index substrate. Both red- and blue-resonance spectral shifts are feasible with either addition of oxide on top, and/or selective etching of the BOX layer below. The simulated results also agree reasonably well with experimental results.

References

[1] S. Boutami, B. Benbakir, X. Letartre, J. L. Leclercq, P. Regreny, and P. Viktorovitch, "Ultimate vertical Fabry–Perot cavity based on single-layer photonic crystal mirrors," *Opt. Express*, vol. 15, pp. 12443–12449, 2007.

[2] M. Sagawa, S. Goto, K. Hosomi, T. Sugawara, T. Katsuyama, and Y. Arakawa, "40-Gbit/s operation of ultracompact photodetector-integrated dispersion compensator based on one-dimensional photonic crystals," *Jpn. J. Appl. Phys.*, vol. 47, pp. 6672–6674, 2008.

[3] A. Chutinan, N. P. Kherani, and S. Zukotynski, "High-efficiency photonic crystal solar cell architecture," *Opt. Express*, vol. 17, pp. 8871–8878, 2009.

[4] O. Kilic, M. Digonnet, G. Kino, and O. Solgaard, "External fibre Fabry–Perot acoustic sensor based on a photonic-crystal mirror," *Meas. Sci. Technol.*, vol. 18, pp. 3049–3054, 2007.

[5] U. Fano, "Effects of configuration interaction on intensities and phase shifts," *Phys. Rev. B*, vol. 124, pp. 1866–1878, 1961.

[6] R. Magnusson and S. S. Wang, "New principle for optical filters," *Appl. Phys. Lett.*, vol. 61, pp. 1022–1024, 1992.

[7] S. Fan and J. D. Joannopoulos, "Analysis of guided resonances in photonic crystal slabs," *Phys. Rev. B*, vol. 65, p. 235112, 2002.

[8] D. K. Jacob, S. C. Dunn, and M. G. Moharam, "Flat-top narrow-band spectral response obtained from cascaded resonant grating reflection filters," *Appl. Opt.*, vol. 41, pp. 1241–1245, 2002.

[9] S. T. Thurman and G. M. Morris, "Controlling the spectral response in guided-mode resonance filter design," *Appl. Opt.*, vol. 42, pp. 3225–3233, 2003.

[10] C. F. R. Mateus, M. C. Y. Huang, L. Chen, C. J. Chang-Hasnain, and Y. Suzuki, "Broadband mirror (1.12–1.62 μm) using single-layer subwavelength grating," *IEEE Photon. Technol. Lett.*, vol. 16, no. 7, pp. 1676–1678, Jul. 2004.

[11] W. Suh and S. Fan, "All-pass transmission or flattop reflection filters using a single photonic crystal slab," *Appl. Phys. Lett.*, vol. 84, pp. 4905–4907, 2004.

[12] S. Boutami, B. B. Bakir, H. Hattori, X. Letartre, J. L. Leclercq, P. Rojo-Romeo, M. Garrigues, C. Seassal, and P. Viktorovitch, "Broadband and compact 2-D photonic crystal reflectors with controllable polarization dependence," *IEEE Photon. Technol. Lett.*, vol. 18, no. 7, pp. 835–837, Apr. 1, 2006.

[13] Y. Ding and R. Magnusson, "Resonant leaky-mode spectral-band engineering and device applications," *Opt. Express*, vol. 12, pp. 5661–5674, 2004.

[14] M. L. Wu, Y. C. Lee, C. L. Hsu, Y. C. Liu, and J. Y. Chang, "Experimental and theoretical demonstration of resonant leaky-mode in grating waveguide structure with a flattened passband," *Jpn. J. Appl. Phys.*, vol. 46, pp. 5431–5434, 2007.

[15] H. Yang, S. Chuwongin, Z. Qiang, L. Chen, H. Pang, Z. Ma, and W. Zhou, "Resonance control of membrane reflectors with effective index engineering," *Appl. Phys. Lett.*, vol. 95, p. 023110, 2009.